Kinetics and Mechanism of the Lamellar to Gyroid Inverse Bicontinuous Cubic Phase Transition

ARTICLE *in* LANGMUIR · AUGUST 2002

Impact Factor: 4.46 · DOI: 10.1021/la0259555

3 AUTHORS:

Adam Squires
University of Reading
43 PUBLICATIONS **793** CITATIONS
SEE PROFILE

Richard H Templer
Imperial College London
129 PUBLICATIONS **5,932** CITATIONS
SEE PROFILE

John M Seddon
Imperial College London
176 PUBLICATIONS **4,911** CITATIONS
SEE PROFILE

Kinetics and Mechanism of the Lamellar to Gyroid Inverse Bicontinuous Cubic Phase Transition

Adam M. Squires,* R. H. Templer, and J. M. Seddon

Department of Chemistry, Imperial College of Science, Technology, and Medicine, London SW7 2AY, U.K.

J. Woenckhaus and R. Winter

University of Dortmund, Department of Chemistry, Physical Chemistry I, Otto-Hahn Strasse 6, D-44227 Dortmund, Germany

S. Finet and N. Theyencheri

European Synchrotron Radiation Facility, BP 220, F-38043 Grenoble Cedex, France

Received May 16, 2002

In this paper, we present data on the transition from the lamellar (L_α) to the gyroid inverse bicontinuous cubic (Q_{II}^G) mesophase. The system investigated was 2:1 lauric acid (LA)/dilauroylphosphatidylcholine (DLPC), at a fixed overall hydration of 50% water by weight. The phase transition was induced by a pressure jump and monitored by time-resolved X-ray diffraction (TRXRD). We observe the gradual appearance of signals from the emergent Q_{II}^G phase and an accompanying disappearance of signals from the initial L_α phase. These changes correspond to a transformation occurring over a time scale which varies between seconds and minutes. We further observe that the lattice parameters of both the initial L_α and final Q_{II}^G phases change throughout the transformation. We suggest that this reflects a competition between the two phases for the limited amount of water available. In addition, we suggest a mechanism whereby the transformation from L_α to Q_{II}^G proceeds via an intermediate phase, which we suggest is the diamond inverse bicontinuous cubic phase (Q_{II}^D). We present evidence for its identity and suggest mechanistic pathways for its formation from the L_α phase and subsequent transformation into the Q_{II}^G phase.

I. Introduction

When amphiphilic lipid molecules are mixed with water, they self-assemble to form lyotropic liquid crystals exhibiting a rich variety of mesophase structures. Some of these structures are made from lipid bilayers, the basic structural element of biological membranes. These include the lamellar and inverse bicontinuous cubic phases.

Inverse bicontinuous cubic (Q_{II}) phases consist of a single lipid bilayer on either side of which lie two interpenetrating continuous networks of water channels. In each phase, the bilayer midplane lies on a mathematical surface known as a triply periodic minimal surface (TPMS). Lipid systems form three Q_{II} phases. These are based on the Schwarz primitive (P), Schwarz double diamond (D), and Schoen gyroid (G) triply periodic minimal surfaces. They are therefore known as the Q_{II}^P, Q_{II}^D, and Q_{II}^G phases and have crystallographic space groups $Im3m$, $Pn3m$, and $Ia3d$, respectively.

Inverse bicontinuous cubic phases have been found to perform a number of biological roles,[1] and it is thought that the mechanism of their formation from the lamellar phase has much in common with the mechanism of membrane fusion and fission.[2−4]

The structures of inverse bicontinuous phases are of technological interest because they have very specific and controllable water channel sizes and a large membrane area. These properties give rise to the use of Q_{II} phases in a number of recent applications, including protein crystallization[5] and drug delivery,[6] and offer potential roles in ultrafiltration and biosensors.[7]

The data presented here were obtained using a sample at a limited hydration of 50 wt % water, below excess-water conditions. This makes the experiment less suitable as a model for membrane transformations in biological systems, which effectively occur in excess water. However, in many of the technological applications of Q_{II} phases, it is precisely this limited hydration which allows us control over the properties described above. The work described here is therefore a model for the formation of such a fixed-hydration Q_{II} phase.

Much work has been done on the thermodynamic properties of Q_{II} phases,[8,9] and they have been modeled using a number of different theoretical approaches,

* Current address for corresponding author: Polymer and Colloids group, Cavendish Laboratory, University of Cambridge, Madingley Road, Cambridge CB3 0HE, U.K.

(1) Lindblom, G.; Rilfors, L. *Biochim. Biophys. Acta* **1989**, *988*, 221−256.
(2) Seddon, J. M. *Biochim. Biophys. Acta* **1990**, *1031* (1), 1−69.
(3) Siegel, D. P.; Banschbach, J. L. *Biochemistry* **1990**, *29* (25), 5975−5981.
(4) Ellens, H.; Siegel, D. P.; Alford, D.; Yeagle, P. L.; Boni, L.; Lis, L. J.; Quinn, P. J.; Bentz, J. *Biochemistry* **1989**, *28*, 3692−3703.
(5) Caffrey, M. *Curr. Opin. Struct. Biol.* **2000**, *10*, 486−497.
(6) Drummond, C. J.; Fong, C. *Curr. Opin. Colloid & Interface Sci.* **2000**, *4*, 449−456.
(7) *Biomolecular self-assembling materials*; Report; National Academy of Sciences: Washington, DC, 1996.
(8) Chung, H.; Caffrey, M. *Nature* **1994**, *368*, 224−226.
(9) Templer, R. H. *Curr. Opin. Colloid & Interface Sci.* **1998**, *3* (3), 255−263.

10.1021/la0259555 CCC: $22.00
Published on Web 08/16/2002

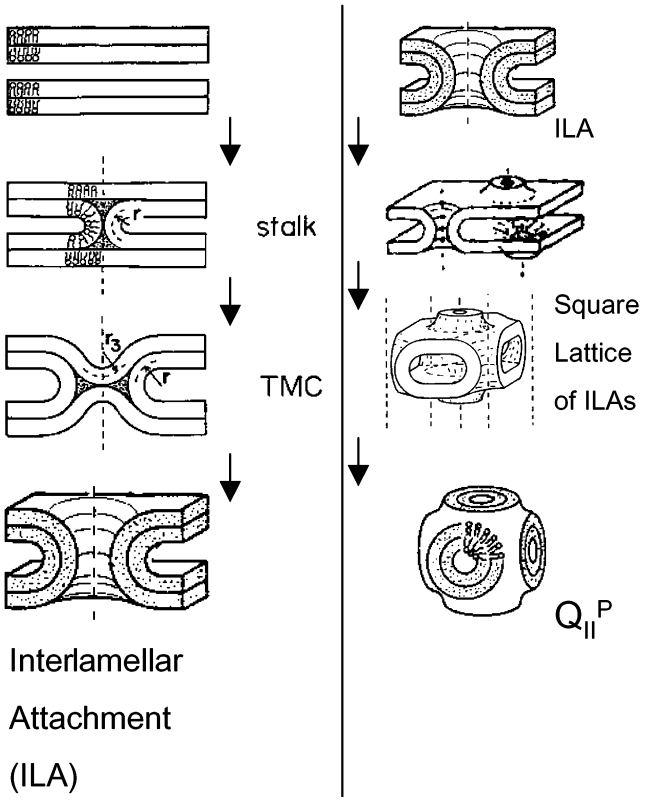

Figure 1. Left: Proposed mechanism for the formation of an interlamellar attachment (ILA) via a stalk and a trans-monolayer contact (TMC). Taken from ref 14. Right: Square lattices of ILAs can readily form the Q_{II}^P phase. Taken from ref 3.

initially considering curvature elastic energy[10,11] and more recently using Lattice−Boltzmann[12] and molecular dynamics[13] simulations. Despite this, and despite the potential biological and technological interest of Q_{II} phases, only very little experimental data are available on the kinetics and mechanism of their formation via a lamellar−Q_{II} transition.

Siegel[3,14,15] has suggested that the transformation from a lamellar to a Q_{II} structure might proceed through the formation of interlamellar attachments (ILAs). These are hollow water-filled necks connecting adjacent bilayers in the lamellar phase. ILAs are in fact identical to fusion pores, which are formed as intermediates in membrane fusion. The mechanism and energetics of their formation have therefore been the subject of much theoretical work.[16−18] The proposed mechanism for the formation of an ILA is shown in Figure 1.

Siegel suggests that ILAs arrange themselves into square arrays, and these arrays stack into primitive lattices which can easily rearrange into the Q_{II}^P inverse bicontinuous cubic phase, as shown in Figure 1. Indeed, images have been obtained using electron microscopy which show square lattices of ILAs.[4,15] The Q_{II}^P phase may then be converted into either a Q_{II}^D or Q_{II}^G phase through a continuous transformation, since their underlying TPMSs have the same topology.[19−21]

Work has been done on the analogous lamellar to gyroid bicontinuous cubic transformation in type I systems. Well-defined epitaxial relationships have been observed between aligned lamellar and Q_I^G mesophases,[22−24] where it appears that the (211) planes of the Q_I^G lie parallel to the (001) lamellar planes. Evidence for the same epitaxial relationship in some type II systems arises from work on aligned samples.[25]

Funari and co-workers[26] have investigated a L_α to Q_{II}^G transition in a ternary phosphocholine/polyoxyethylene/water system, and they suggest that this time there is an epitaxial relationship between the (220) planes of the Q_{II}^G phase and the (001) L_α planes. However, their experiments were not performed on aligned samples, and the epitaxy which they determined was based only on the ratio of lattice parameters.

Little time-resolved work is available for the lamellar−bicontinuous cubic transition in type II systems,[27−29] but results indicate that the kinetics of the process are generally slow, of the order of tens of minutes, and the phase transition is associated with considerable hysteresis. Much faster phase transitions, of the order of seconds, have been observed for the type I transformation.[30]

The lipid system under investigation is a 2:1 fatty acid/PC mixture of 2LA/DLPC. The temperature−water content phase behavior of this system at atmospheric pressure has been well characterized experimentally[31] and the subject of theoretical modeling.[10,11] We have already published work on the pressure−temperature phase behavior of 2LA/DLPC/50 wt % water.[32] At this water content, the system forms a range of equilibrium mesophase structures, including L_α, H_{II}, Q_{II}^G, and Q_{II}^D. The work also included time-resolved data on the transformations from Q_{II}^G to Q_{II}^D and from Q_{II}^D to $Q_{II}^D + H_{II}$ + excess water.

II. Materials and Methods

A. Sample Preparation. The system under investigation was a mixture of dilauroylphosphatidylcholine (DLPC) and lauric acid (LA) in the molar ratio 2:1 LA/DLPC, hydrated to 50 wt %

(10) Templer, R. H.; Seddon, J. M.; Duesing, P. M.; Winter, R.; Erbes, J. *J. Phys. Chem. B* **1998**, *102* (37), 7262−7271.
(11) Schwarz, U. S.; Gompper, G. *Langmuir* **2001**, *17*, 2084−2096.
(12) Nekovee, M.; Coveney, P. V. *J. Am. Chem. Soc.* **2001**, *123*, 12380−12382.
(13) Marrink, S. J.; Tieleman, D. P. *J. Am. Chem. Soc.* **2001**, *123*, 12383−12391.
(14) Siegel, D. P.; Epand, R. M. *Biophys. J.* **1997**, *73* (6), 3089−3111.
(15) Siegel, D. P.; Burns, J. L.; Chestnut, M. H.; Talmon, Y. *Biophys. J.* **1989**, *56* (1), 161−169.
(16) Kozlovsky, Y.; Kozlov, M. M. *Biophys. J.* **2002**, *82*, 882−895.
(17) Kozlov, M. M.; Leikin, S. L.; Chernomordik, L. V.; Markin, V. S.; Chizmadzhev, Y. A. *Eur. Biophys. J.* **1989**, *17*, 121−129.
(18) Siegel, D. P. *Biophys. J.* **1999**, *76*, 291−313.
(19) Sadoc, J. F.; Charvolin, J. *Acta Crystallogr., Sect. A* **1989**, *45* (Jan), 10−20.
(20) Fogden, A.; Hyde, S. T. *Eur. Phys. J. B:* **1999**, *7*, 91−104.
(21) Benedicto, A. D.; O'Brien, D. F. *Macromolecules* **1997**, *30*, 3395−3402.
(22) Rancon, Y.; Charvolin, J. *J. Phys. Chem.* **1988**, *92* (9), 2646−2651.
(23) Kekicheff, P.; Cabane, B. *Acta Crystallogr., Sect. B* **1988**, *44* (4), 395−406.
(24) Clerc, M.; Levelut, A. M.; Sadoc, J. F. *J. Phys. II* **1991**, *1*, 1263−1276.
(25) Templer, R. H.; Warrender, N. A.; Meadows, R.; Seddon, J. M. In *The structure and conformation of amphiphilic membranes*; Lipowsky, R., Richter, D., Kremer, K., Eds.; Springer-Verlag: Berlin 1992; pp 230−233.
(26) Funari, S. S.; Mädler, B.; Rapp, G. *Eur. Biophys. J.* **1996**, *24*, 293−299.
(27) Erbes, J.; Czeslik, C.; Hahn, W.; Winter, R.; Rappolt, M.; Rapp, G. *Ber. Bunsen-Ges. Phys. Chem.* **1994**, *98* (10), 1287−1293.
(28) Qiu, H.; Caffrey, M. *Biomaterials* **2000**, *21*, 223−234.
(29) Caffrey, M.; Cheng, A. *Curr. Opin. Struct. Biol.* **1995**, *5*, 548−555.
(30) Clerc, M.; Laggner, P.; Levelut, A.-M.; Rapp, G. *J. Phys. II* **1995**, *5*, 901−917.
(31) Templer, R. H.; Seddon, J. M.; Warrender, N. A.; Syrykh, A.; Huang, Z.; Winter, R.; Erbes, J. *J. Phys. Chem. B* **1998**, *102* (37), 7251−7261.
(32) Squires, A. M.; Seddon, J. M.; Templer, R. H. *Langmuir* **2000**, *16*, 3578−3582.

water. The LA and DLPC were obtained from Avanti Polar Lipids (Alabaster, AL) and Fluka, respectively, each at >99% purity, according to the manufacturers. The purities of both lipids were confirmed by thin-layer chromatography. The lipids were left overnight in a desiccator before use to remove residual moisture. The 2LA/DLPC mixture was prepared by codissolving the appropriate ratio of LA and DLPC in cyclohexane (BDH chemical supplies, Dorset, U.K.) and removing the solvent by freezing to liquid nitrogen temperature and then freeze-drying overnight. To this was added an equal mass of Millipore-filtered distilled water, and this mixture was incubated overnight at 42 °C, approximately 10 °C above the chain melting temperature. It was then allowed to cool, before being homogenized. Homogenization was achieved by using a centrifuge to force the sample backward and forward through a 1-mm diameter hole in a Teflon "hourglass". The sample was centrifuged through this device approximately 10 times until it appeared homogeneous upon visual inspection.

B. Sample Cell. The experiments employed a high-pressure cell with flat diamond windows of thickness 0.7 mm, which was designed and built at the University of Dortmund. The samples were placed in the pressure cell in Teflon rings of thickness 1 mm, with Kapton windows held on with double-sided sticky tape. The cell is suitable for studies up to pressures of 5 kbar and temperatures up to 140 °C with accuracies of ±5 bar and ±0.2 °C. The pressure jump which induced the L_α to Q_{II}^G transition was triggered by the computer-controlled opening of an air-operated valve. This allowed a rapid jump in pressure; the cell can achieve pressure jumps of up to 1 kbar in under 7 ms, which is much faster than the time scale of the transformation (from seconds to minutes; see section IIIC). No adiabatic temperature change was detected in these experiments within the accuracy of our temperature measurements (±0.2 °C). Further details of the apparatus are provided elsewhere.[33]

C. X-ray Beamline. Experiments at the European Synchrotron Radiation Facility (ESRF) were performed at the high-brilliance beamline ID02 (experiment LS1560). Details of beam and detector specifications can be found at the ESRF website.[45] The experiments were carried out using a beam of approximate wavelength $\lambda = 1.0$ Å, with dimensions 0.46 mm × 0.15 mm and a typical flux of 8×10^{12} photons per second. Two-dimensional diffraction patterns were recorded on a detector consisting of a Thomson X-ray intensifier (TH 49-427) lens coupled to the ESRF-developed FReLoN CCD camera. This detector had an active area of size 230 mm and a frame rate of 10 images (1024×1024 pixels^2) per second with a nominal dynamic range of 14 bits. The sample−detector distance was set to 2.000 m. Intensity data were normalized to compensate for fluctuations in beam intensity.

D. Time-Resolved Acquisition. Time-resolved X-ray diffraction data were obtained as a sequence of exposures, each of duration 0.1 s, with a delay between successive exposures. The delay was increased throughout the data acquisition, following a geometric progression of the form $t_n = t_1 a^{n-1}$, where t_n is the delay following exposure number n; our experiments used an initial delay of $t_1 = 0.1$ s and typically a common ratio of $a = 1.2$ or 1.25.

Such a timing sequence takes exposures more rapidly earlier on in the phase transition and progressively less frequently as time progresses. This enables us to monitor changes over a range of time scales.

E. X-ray Diffraction Pattern Analysis. The CCD camera recorded 2-D diffraction patterns. As the samples were powder-like, each took the form of a series of concentric rings. Representative diffraction patterns from the Q_{II}^G and L_α phases are shown in Figure 2.

The center of the beam was located using software developed in-house. Each diffraction pattern was then integrated radially about this position to give an average pixel intensity as a function of distance from the beam center, in the form of a 1-D diffraction pattern. We can convert values for the position of a reflection in pixels into a d spacing, using values for sample−detector distance (l), wavelength (λ), and pixel size (p) of $l = 2000$ mm, $\lambda = 0.9887$ Å, and $p = 0.173$ mm.

(33) Erbes, J.; Winter, R.; Rapp, G. *Phys. Chem. Chem. Phys.* **1996**, *100* (10), 1713−1722.

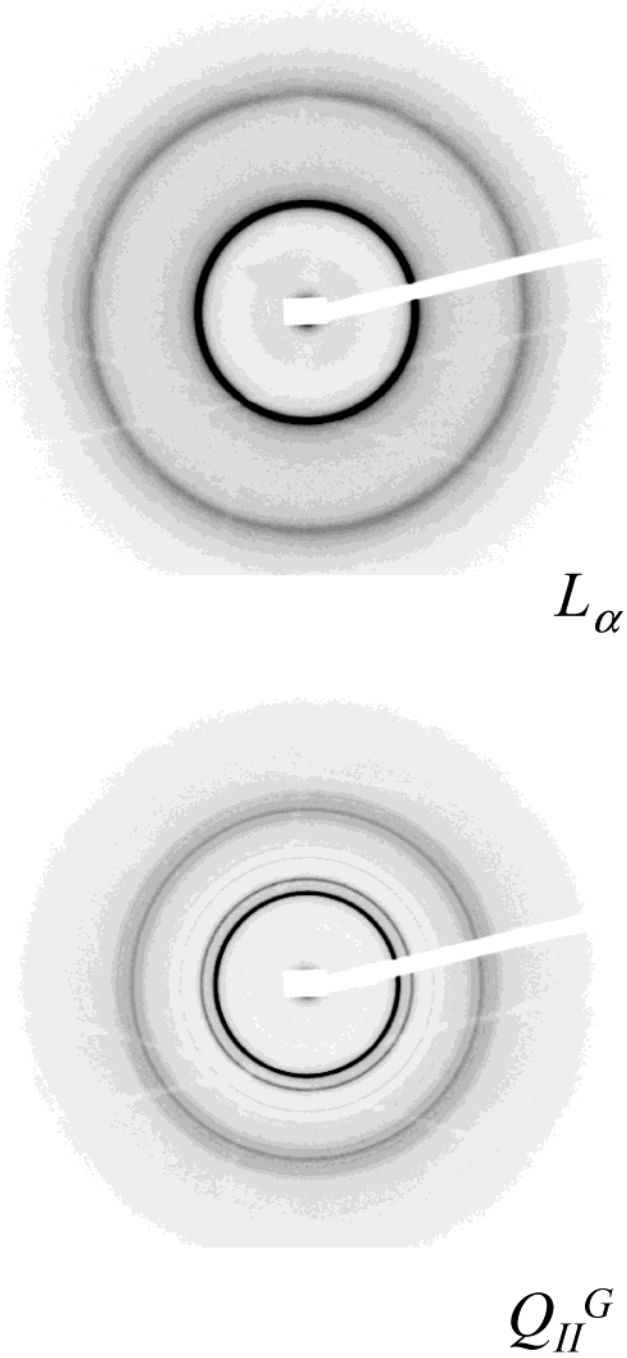

Figure 2. Representative 2-D diffraction patterns for the L_α and Q_{II}^G phases. A very faint ring from the L_α (100) reflection remains in the Q_{II}^G diffraction pattern.

For ease of visualization, we have taken all of the 1-D diffraction patterns from a single pressure jump experiment and displayed them displaced vertically to give a "stacked" plot, as shown in Figure 4. For greater clarity, the intensity axis is displayed on a logarithmic scale.

III. Results and Discussions

A. Phase Behavior of 2LA/DLPC/50 wt % Water. The pressure−temperature phase diagram for the system showing the lamellar and Q_{II}^G phases is shown in Figure 3. (Other Q_{II} and H_{II} phases occur at the lower pressure/higher temperature region of the phase diagram; these

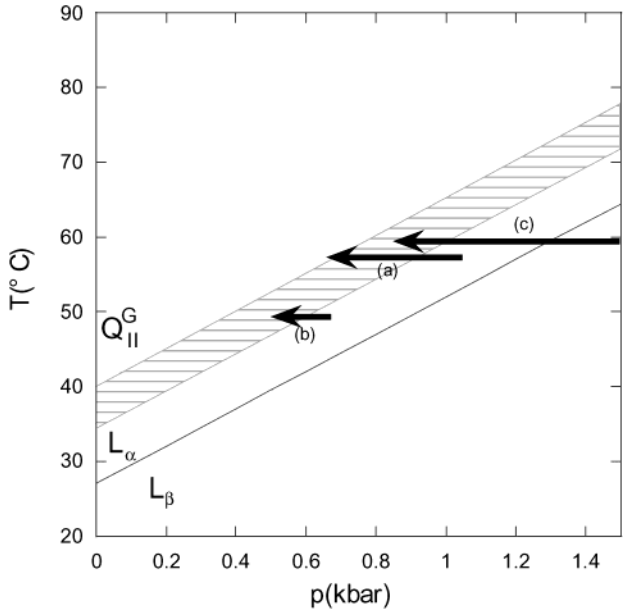

Figure 3. Pressure−temperature phase diagram for 2LA/DLPC.

did not feature in the work described in this paper and, for this reason, have not been included.) The position of the L_β/L_α phase boundary was taken from static measurements in excess water, from Winter et al.[34] The boundaries of the L_α/Q_{II}^G coexistence region were estimated using atmospheric-pressure measurements carried out at Imperial College on the 2LA/DLPC/50 wt % water sample, and assuming that these phase boundaries also have a slope of approximately 25 °C kbar^{-1}.[34] This was confirmed by static measurements taken at ESRF from 2000 bar down to 200 bar at intervals of 200 bar.

B. Overview of Time-Resolved Data. Three pressure jump experiments were carried out. The start and end conditions for the pressure jumps have been shown as arrows on the phase diagram shown in Figure 3. "Stacked" plots generated from the data from each pressure jump experiment are shown in Figure 4, with parts a−c corresponding to arrows a−c in Figure 3.

Figure 4a shows a complete transformation from lamellar to Q_{II}^G, with a number of interesting features. The system begins in the L_α phase. Following the pressure jump, the two peaks from the L_α phase gradually disappear. At the same time, another set of peaks appears and develops into those corresponding to the Q_{II}^G phase. Accompanying this change is a shift in both phases toward a higher angle, corresponding to a smaller lattice parameter. In addition, the first seven spectra show an extra signal to the low-angle side of the emerging $\sqrt{6}$ Q_{II}^G reflection. Figure 4b shows a pressure jump carried out under different conditions, this time ending with coexisting L_α and Q_{II}^G phases. Again, we see the shift to a smaller lattice parameter in the L_α phase, although not in the Q_{II}^G phase. The whole process occurs over a much longer time scale than that in experiment a. The low-angle intermediate signals are now stretched out over more exposures, allowing us to investigate them more closely. This is described more fully in section IIIE.

Finally, Figure 4c shows a similar jump, again to coexisting L_α and Q_{II}^G phases, but has an unusual appearance at the start. This is because the system begins

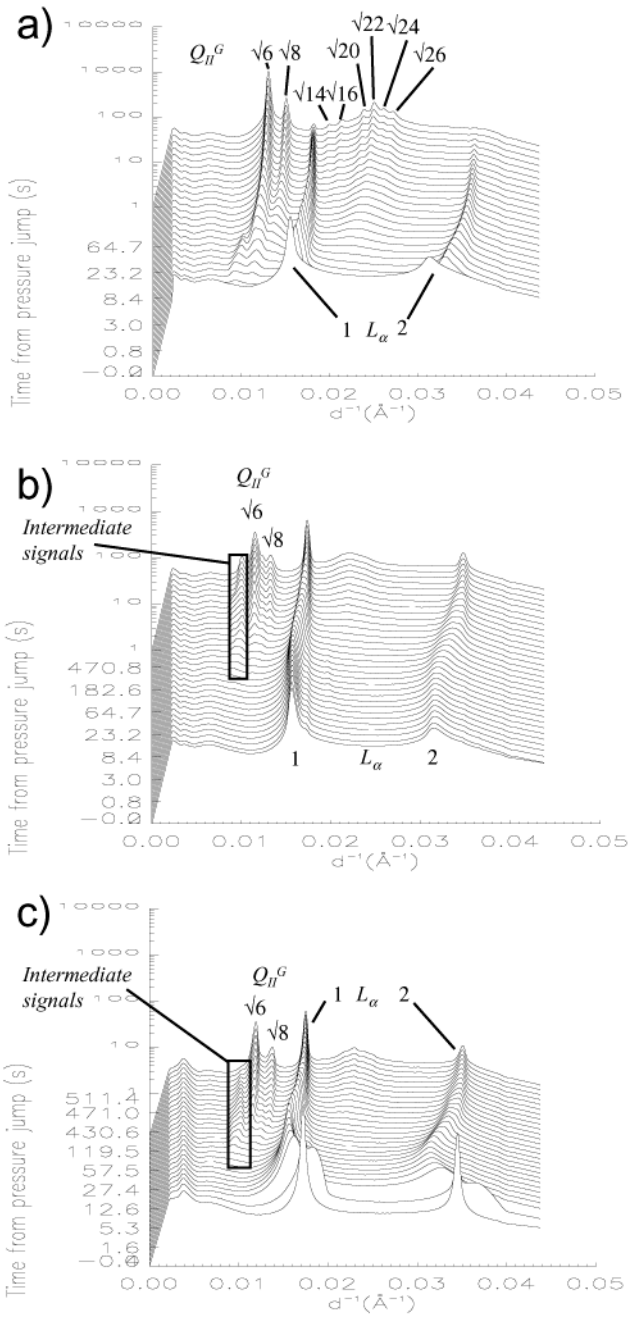

Figure 4. "Stacked" plots showing lamellar to Q_{II}^G transitions. The conditions employed for the pressure jump experiments were as follows: (a) $T = 57.5$ °C, $P = 1030-660$ bar; (b) $T = 49.5$ °C, $P = 660-500$ bar; (c) $T = 59.5$ °C, $P = 1490-850$ bar.

in the L_β rather than the L_α phase (see Figure 3). The effects which this difference has on the observed behavior will be discussed more fully in section IIIF. The low-angle intermediate signals seen in the other two pressure jumps are also observed here.

C. Time Scales. To quantify the "time scale" of each transformation, the integrated (200) peak intensity of the L_α phase was monitored as a function of time. The graphs obtained are shown in Figure 5.

A monoexponential or biexponential decay was fitted to the data. (Biexponential curves were chosen where the data did not give a good fit to monoexponential behavior.) It is important to note that no physical significance was assumed when choosing these fits, and they were employed merely as a way of quantifying the time scale of the transformation. We have done this by defining a parameter

(34) Winter, R.; Erbes, J.; Templer, R. H.; Seddon, J. M.; Syrykh, A.; Warrender, N. A.; Rapp, G. *Phys. Chem. Chem. Phys.* **1999**, *1*, 887−893.

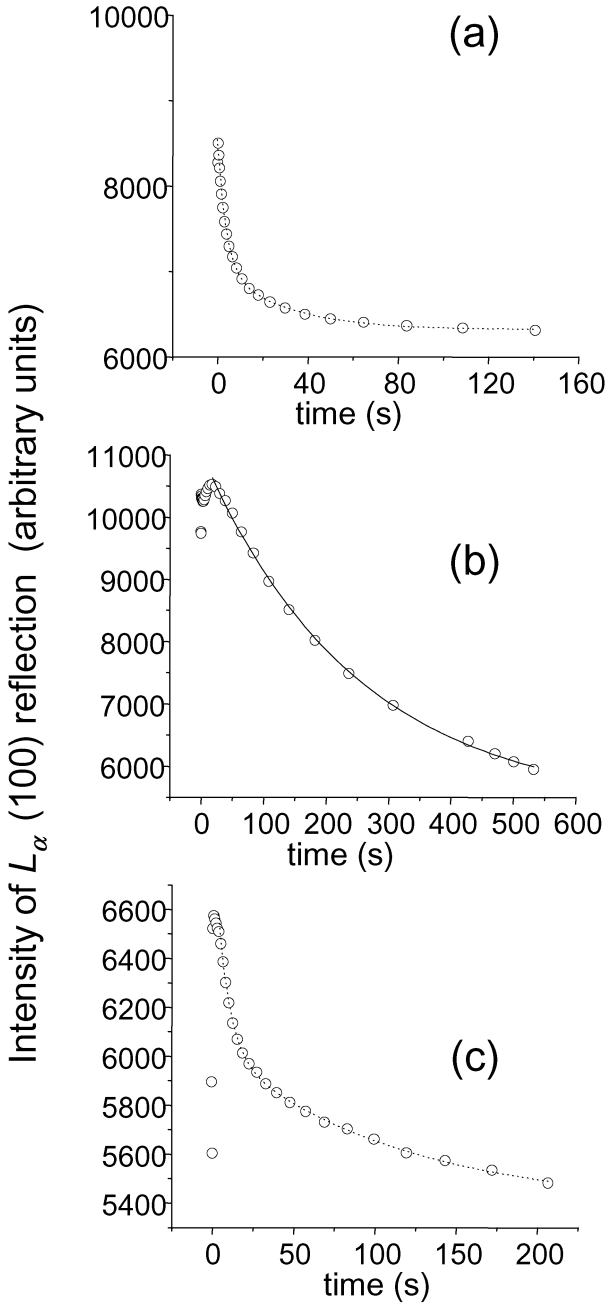

Figure 5. Changes in L_α-integrated peak intensity with time (open circles) and curve fits, some monoexponential (solid lines) and some biexponential (dotted lines). Graphs a−c correspond to data from experiments a−c in Figures 3 and 4, respectively. The initially low values for the integrated peak intensity in plot c probably reflect the different scattering behavior of the L_β phase as compared with the L_α phase.

τ as the time at which the integrated peak intensity is halfway toward its final value, to give an idea of the time scales involved. Values of τ are quoted in Table 1.

Table 1 shows that the time scale for the transformation can vary from seconds to minutes, depending on the temperature and pressure jump employed. However, the conditions, starting and ending pressures, temperature, initial phase, and sample history, vary too much to allow a systematic comparison and therefore a study of the effect of any one of these variables. Moreover, monoexponential or biexponential curve fits must at best be an approximation to what is clearly a more complex kinetic behavior.

D. Lattice Parameters and Water Contents. All three pressure jump data sets show the same trend, that

Table 1. Values for the "Half-time" (τ) for Changes in Lamellar-Integrated Peak Intensities, Calculated from Data Shown in Figure 5[a]

experiment	a	b	c
T (°C)	57.5	49.5	59.5
pressure jump (bar)	1030−660	660−500	1490−850
τ	4.27	193	22.0

[a] Values for τ are quoted in units of seconds, with an error of ±1%, determined by the curve-fitting software from the goodness of fit.

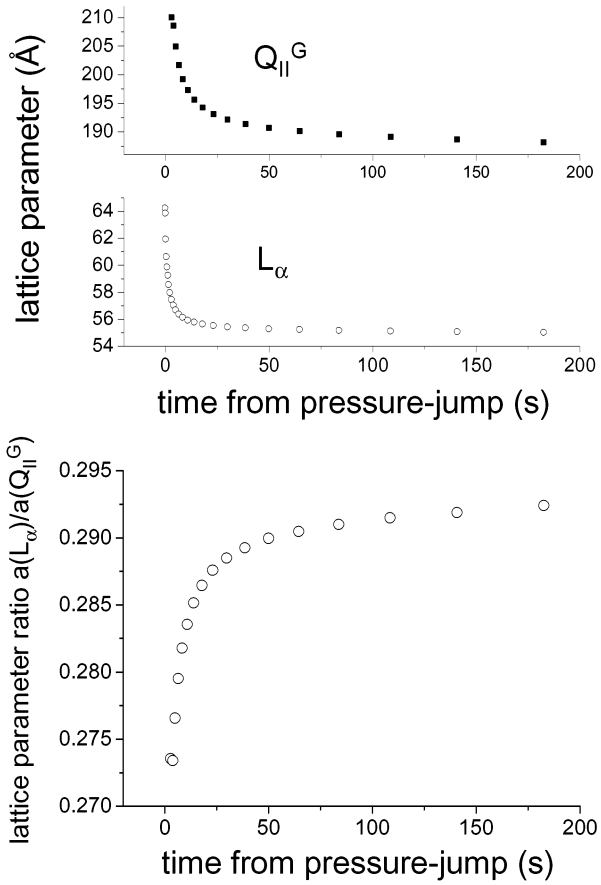

Figure 6. Lattice parameters (top) and lattice parameter ratios (bottom) of L_α and Q_{II}^G phases.

the emergence of the Q_{II}^G phase is accompanied by a move to a lower lattice parameter of the L_α phase. At later stages in the transformation, Figure 4a, the lattice parameter of the Q_{II}^G phase itself decreases. In this section, we examine the data from pressure jump experiment a in more detail in an attempt to account for these changes.

As a preliminary analysis, we can calculate the ratio of lattice parameters $a(L_\alpha)/a(Q_{II}^G)$ throughout the transformation. We note that in other work[26] it has been suggested that a correlation of peak positions between two phases, and therefore a ratio of lattice parameters, may be taken as evidence of an epitaxial relation. A plot of the lattice parameter ratio throughout the transformation is shown in Figure 6.

Suggested epitaxial relations for this transformation relate the (001) plane of the L_α phase either to the (220) plane[26] or to the (211) plane[25] of the Q_{II}^G phase. These would suggest a lattice parameter ratio of $a(L_\alpha)/a(Q_{II}^G) = 1/\sqrt{8} = 0.354$ or $1/\sqrt{6} = 0.408$, respectively. The lattice parameter ratio shown in Figure 6 falls significantly below either value. Moreover, its value is not constant but varies throughout the transformation. We do not present this as

evidence against either suggested epitaxy; rather, we suggest that in this case the lattice parameter data do not reflect the epitaxial route taken. Instead, we attempt to account for the lattice parameter data in terms of mesophase water contents.

The water content of each phase may be calculated from the lattice parameter, given certain parameters which reflect the molecular geometry of the lipid molecules involved. The calculations assume that there is a part of the lipid molecule which does not alter in cross-sectional area during isothermal bending. This is known as the "pivotal surface".[35,36] The cross-sectional area per lipid at this surface and the molecular volume between this surface and the ends of the hydrophobic chains are given by A_n and v_n, respectively. The lipid geometry is characterized by these two parameters and by the total molecular volume of the lipid, v. In this case, the "lipid molecule" is in fact a unit consisting of 1 DLPC and 2 LA molecules.

A_n and v_n have already been determined for 2LA/DLPC by fitting data of the lattice parameter as a function of the water volume fraction. They have been found to take values of $v_n = 1230 \pm 30$ Å^3 and $A_n = 108 \pm 2$ Å^2.[31] The total molecular volume, v, has also been obtained from density measurements and found to take a value of 1735 Å^3.

Given these values of v, v_n, and A_n, it is possible to calculate the water volume fraction contained within the mesophase, ϕ_w, from its lattice parameter, a. For the lamellar phase, the bilayer thickness is simply $2v/A_n$. The water volume fraction in the lamellar phase is thus given by

$$\phi_w^L = 1 - \frac{2v}{A_n a} \quad (1)$$

For the Q_{II}^G phase, more complex mathematics are involved. Assuming a geometry where the pivotal surface lies parallel to the underlying periodic minimal surface, we may use differential geometry to derive the following relationship.[31]

$$\left(\frac{A_n}{v}\right)^3 a^3 + 6\sigma_0\left(\frac{A_n}{v}\right)^2 \frac{a^2}{(1-\phi_w)} - \left[\frac{36\pi\chi}{(1-\phi_w)}\left(\frac{v_n}{v}\right)^2 + \frac{32{\sigma_0}^3}{(1-\phi_w)^3}\right] = 0 \quad (2)$$

Solving this gives the water volume fraction in the Q_{II}^G phase, ϕ_w^G.

$$\phi_w^G = 1 - 4v^3\sigma^3(a^3{A_n}^3v^6\sigma^6 + \sqrt{v^{12}\sigma^9(a^6{A_n}^6\sigma^3 - (a^2{A_n}^2\sigma - 6\pi v{n}^2\chi)^3)})^{1/3}/[a^2{A_n}^2v^4\sigma^4 - 6\pi v^4{v_n}^2\sigma^3\chi + (a^3{A_n}^3v^6\sigma^6 + \sqrt{v^{12}\sigma^9(a^6{A_n}^6\sigma^3 - (a^2{A_n}^2\sigma - 6\pi{v_n}^2\chi)^3)})^{2/3}] \quad (3)$$

For the Q_{II}^G phase, the equation uses the values $\sigma = 3.0910$ and $\chi = -8$ for the dimensionless minimal surface area per unit cell and the Euler characteristic, respectively.

We assume that the lipid geometry and therefore the parameters A_n, v_n, and v remain approximately constant with temperature and pressure. This is borne out by the fact that, within a single-phase region, no significant change in lattice parameters is detected over the temperature and pressure ranges of the experiments.[32]

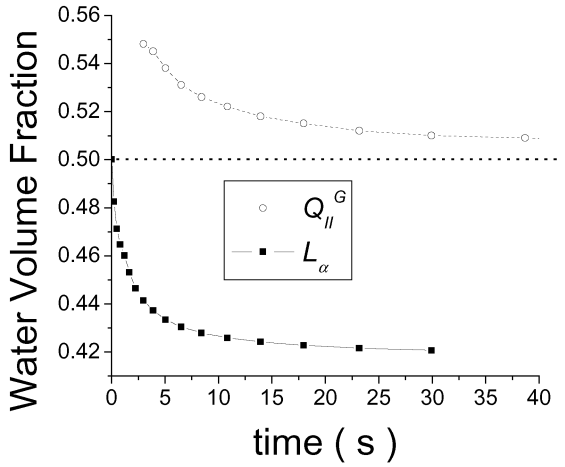

Figure 7. Water volume fractions of the L_α and Q_{II}^G phases as a function of time, calculated from the changing lattice parameters shown in Figure 6, for the first 40 s following pressure jump.

The L_α phase begins at a lattice parameter of $a = 64.23$ Å. From eq 1, we can calculate the water content of the lamellar phase, $\phi_w^L = 0.500 \pm 0.001$. Within error limits, this is the same value as that of the sample overall, showing that the L_α phase does not coexist with excess water. The Q_{II}^G phase begins to form at a lattice parameter of 210 Å. This value decreases toward its final measured lattice parameter after 180 s of $a(Q_{II}^G) = 187.3$ Å. From eq 3, we estimate its water content to be $\phi_w^G = 0.499 \pm 0.001$. Again, this implies that the final Q_{II}^G phase does not coexist with excess water.

For intermediate stages, where the L_α and Q_{II}^G phases coexist, we continue to use eqs 1 and 3 to estimate the water content of each phase. These values are shown in Figure 7.

We note that, in such situations, there exists the possibility of a difference in LA/DLPC ratios between the two phases. In this event, it may not be appropriate to use the same values of A_n, v_n, and v as for a 2:1 mixture. Instead, we could use an approximate model which assumes a constant monolayer thickness, l. For the L_α phase, we would still use eq 1 and take half of the bilayer thickness to give $l = (v/A_n) = 16.1$ Å. For the Q_{II}^G phase, l takes a smaller value, reflecting the curvature of each monolayer. However, we approximate this to having a constant value over a range of Q_{II}^G lattice parameters. The water volume fraction is related to monolayer thickness by the following equation.[31]

$$\phi_w^G = 1 - \left(2\sigma\frac{l}{a} + \frac{4}{3}\pi\chi\left(\frac{l}{a}\right)^3\right) \quad (4)$$

Again, we use the values $\sigma = 3.0910$ and $\chi = -8$ for the dimensionless minimal surface area per unit cell and the Euler characteristic. The monolayer thickness, l, is estimated from values of $a(Q_{II}^G) = 187.3$ Å and $\phi_w^G = 0.499$ to obtain $l = 15.8$ Å. If we use this value of l with eq 4, the approximate estimates of ϕ_w^G obtained agree with the values plotted in Figure 7 to within ±0.001.

Of course, we are still assuming that, in cases where the LA/DLPC ratio deviates from 2:1 in cases of mesophase coexistence, we can still use these values of monolayer thickness to estimate the water content in each phase.

(35) Templer, R. H. *Langmuir* **1995**, *11* (1), 334−340.
(36) Kozlov, M. M.; Leikin, S.; Rand, R. P. *Biophys. J.* **1994**, *67*, 1603−1611.

The two lipid components, however, have the same chain lengths, so we suggest that this approximation is a reasonable one and do not expect our results to be greatly affected by changes in monolayer thickness arising as a result of variations in lipid composition.

We can now use our estimates for water contents to account for the observed changes in lattice parameter. The Q_{II}^G phase begins to form at a water volume fraction of $\phi_w^G = 0.55 \pm 0.01$. As it forms, this higher water content phase sucks the water out of the remaining L_α phase. Eventually, however, there is a limit to how much water is available. To form more and more of the Q_{II}^G phase, the Q_{II}^G phase itself must be of a lower and lower water content. Its final value, as we have shown, is $\phi_w^G = 0.499 \pm 0.001$, corresponding to the overall water content of the sample.

We therefore suggest that the changing lattice parameters reflect a competition between the coexisting L_α and Q_{II}^G phases for a limited amount of water. To provide a quantitative model of this competition, we would need to consider the energy associated with removing water from each phase. In the Q_{II}^G phase, removing water causes the water channels to shrink. The lipid monolayers surrounding the water channels therefore have to bend more, and this therefore increases the bending energy of the system. Quantitatively, this has been directly measured for the 2LA/DLPC system at 42 °C and atmospheric pressure over a range of water contents, using the osmotic stress technique,[37] although the results obtained may be different at $T = 57.5$ °C and $P = 660$ bar. In the L_α phase, the removal of water forces adjacent bilayers closer together. There is an energetic cost to this process, as there is an interaction between the bilayers which causes them to repel one another. This repulsive interaction has a number of contributions, which are discussed more fully in a review by Rand and Parsegian.[38] However, no osmotic stress data are available on 2LA/DLPC in the L_α phase. If such data become available, we suggest that this could provide a quantitative description of the changing lattice parameters of the two phases throughout the transformation described here, and in other phase transitions carried out under limited-hydration conditions.

E. Intermediates. A closer analysis of the data shown in Figure 4 reveals a number of "intermediate" peaks in the same region as the $\sqrt{6}$ Q_{II}^G reflection, especially in parts b and c. Figure 8 shows a region taken from Figure 4c, where this can be seen in more detail. Three separate peaks are present, labeled i, ii, and iii in order of increasing scattering angle. Of these, peak ii is the most well-defined; peak i exists as a shoulder to the small-angle side of peak ii, while peak iii appears as a small hump between the $\sqrt{6}$ and $\sqrt{8}$ reflections of the Q_{II}^G phase.

The fact that these peaks overlap makes their accurate analysis more difficult. The software package "Microcal Origin" was used to fit the whole region containing peaks i, ii, and iii as well as the two Q_{II}^G reflections as a sum of five Lorentzian peaks. The choice of peak shape was made following a similar treatment by Osterberg et al.[39] A sample spectra taken from Figure 8 is shown in Figure 9, together with such a multi-Lorentzian fit.

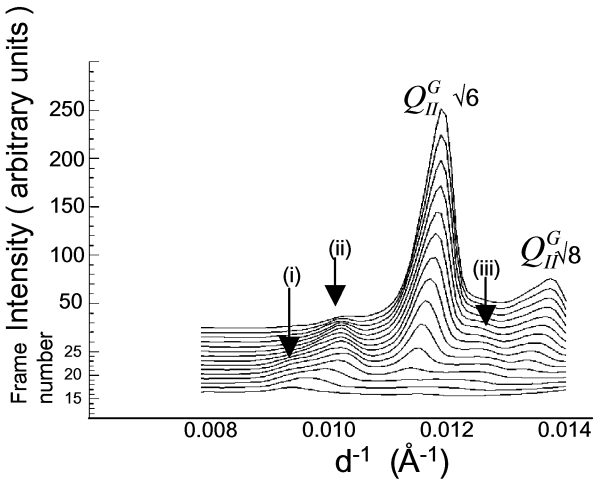

Figure 8. Stacked plots showing intermediate signals. The plots were taken from Figure 4c, between 10 and 100 s after pressure jump.

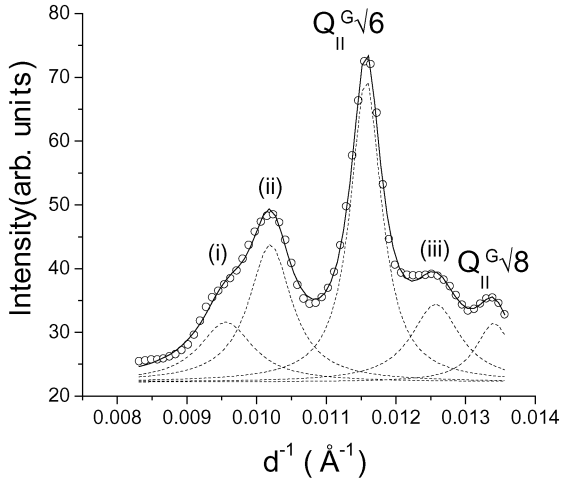

Figure 9. Sample plot with Lorenzian fits. Data are taken from Figure 8 at time $t = 22.6$ s after pressure jump (open circles) and fitted as the sum of five Lorenzian peaks (broken lines).

We can now estimate the positions of the three intermediate reflections for all of the data from the three pressure jump experiments shown in Figure 4 and monitor their appearance and disappearance with time. Data for the positions of the intermediate peaks for all three jumps are shown in Figure 10.

We have calculated the ratio of d spacings of the intermediate peaks in order to determine whether they are signals from the same structure; if two peaks have d spacings in a ratio which remains constant, then it is likely that they are different reflections from the same structure, whereas if the ratio of their d spacings changes, then they must be from different structures.

In all of the data, it was found that the d spacings of peaks ii and iii were in the ratio $d(\text{ii})/d(\text{iii}) = 1.22 \pm 0.1$, which, within experimental error, is $\sqrt{3}/\sqrt{2}$. This ratio was constant for all of the data taken from all three pressure jumps (Figure 11). However, the d spacing of peak i clearly does not vary proportionally with the other two. It therefore appears that peaks ii and iii are from a different species than that which gives rise to the earlier signal i.

We do not have enough data to deduce any information on the identity of the species giving rise to intermediate peak i. However, we can speculate on the identity of the

(37) Squires, A. M.; Seddon, J. M.; Templer, R. H. In *Probing and Modelling Membranes and Proteins*; Templer, R., Leatherbarrow, R., Eds.; R. S. C. Publications, in press.

(38) Rand, R. P.; Parsegian, V. A. *Biochim. Biophys. Acta* **1989**, *988*, 351−376.

(39) Osterberg, F.; Kriechbaum, M.; Polcyn, A.; Skita, V.; Tate, M. W.; So, P. T. C.; Gruner, S. M.; Erramilli, S. *Phys. Rev. Lett.* **1994**, *72* (18), 2967−2970.

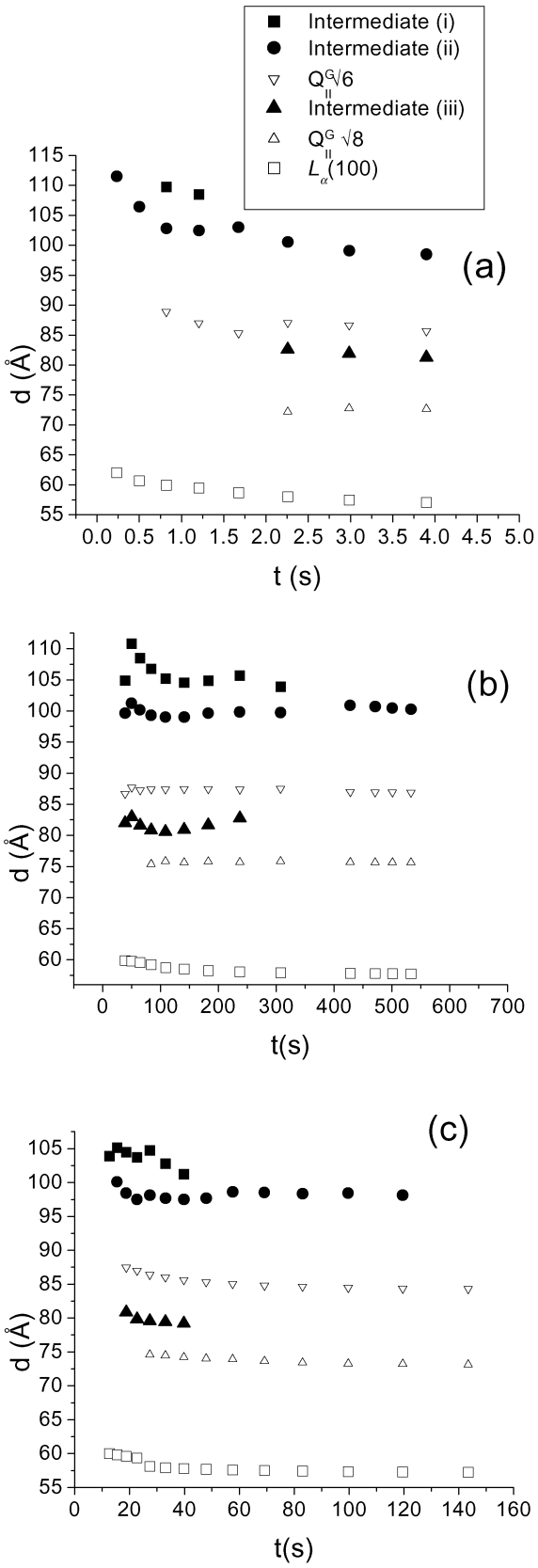

Figure 10. Intermediate peak positions. Plotted are positions of intermediate peaks i, ii, and iii (solid symbols) with positions of peaks from initial L_α and emergent G^G_{II} phases (hollow symbols).

second intermediate, which produces peaks ii and iii. We note that $\sqrt{2}$ and $\sqrt{3}$ are the first two observed reflections of another inverse bicontinuous cubic structure, the Q^D_{II}

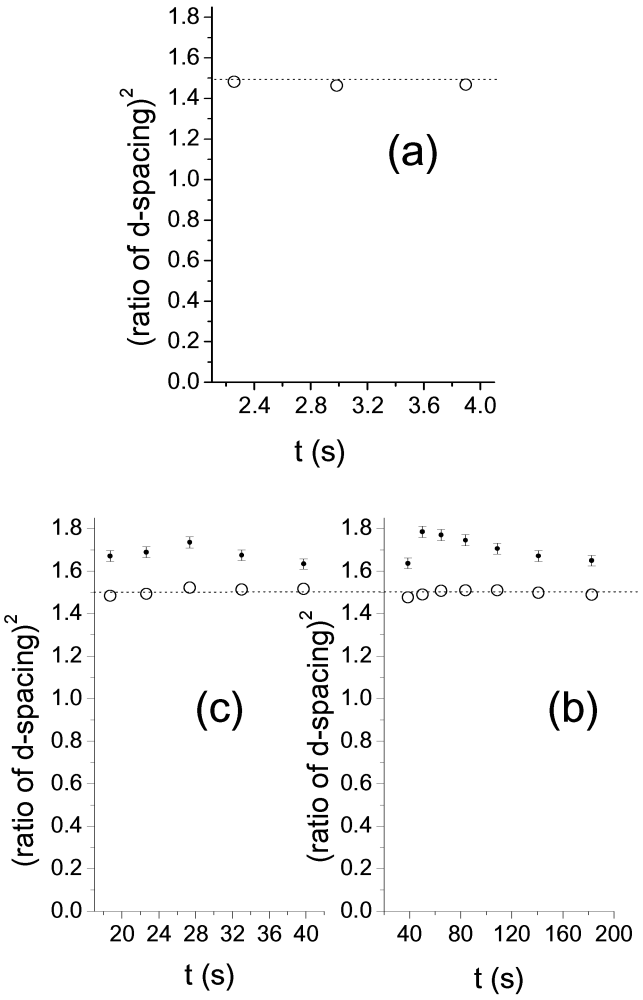

Figure 11. Intermediate peak position ratios. Squares of ratios of *d* spacings are plotted as a function of time for intermediate peaks from the three pressure jump experiments. Solid circles with error bars denote $(d(\text{i})/d(\text{iii}))^2$, and hollow circles $(d(\text{ii})/d(\text{iii}))^2$. The dotted line shows the value $(d(\text{ii})/d(\text{iii}))^2 = {}^3/_2$.

phase, and that they appear in approximately the same intensity ratio. Q^D_{II} itself is an equilibrium phase for 2LA/DLPC/50 wt % water under different conditions, appearing on the high-temperature/low-pressure side of Q^G_{II} in the phase composition diagram.[32] In the remainder of this section, we suggest simple mechanisms for the formation of a Q^D_{II} phase from the L_α phase and its subsequent conversion to the final Q^G_{II} phase.

The Q^D_{II} phase could be formed from the L_α phase by a modified version of the mechanism proposed by Siegel for the formation of a Q^P_{II} phase, described in section I. In this case, the ILAs (interlamellar attachments) joining a given pair of bilayers arrange into a hexagonal rather than a square lattice (compare Figures 1 and 12). In fact, it has been shown[40] that ILAs spanning the same water region would be expected to repel one another. This makes a hexagonal array a more favorable structure than a square one.

Just as in Siegel's proposed mechanism, a Q^P_{II} phase consists of square arrays of ILAs stacked into a primitive lattice, so we can imagine a Q^D_{II} phase to be a stack of hexagonal arrays of ILAs. This may be seen more clearly in the section of minimal surface shown in Figure 13 and also in images shown in ref 13. In the Q^D_{II} phase, the

(40) Charitat, T.; Fourcade, B. *J. Phys. II* **1997**, *7*, 15−35.

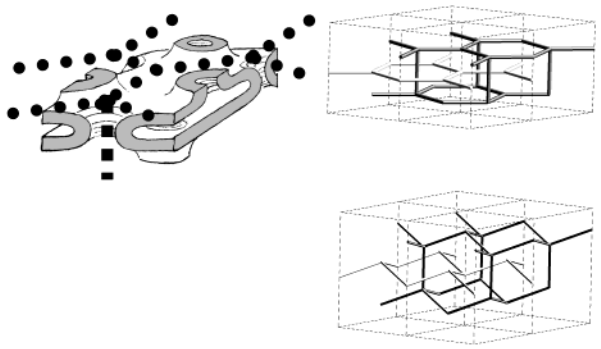

Figure 12. Formation of a Q_{II}^{D} phase from a hexagonal array of interlamellar attachments. A hexagonal array of ILAs (left) gives rise to stacked hexagonal networks of water channels (top right), from which we can imagine a simple rearrangement which gives the Q_{II}^{D} structure (bottom right). The two different networks of water channels are illustrated in different shades for clarity.

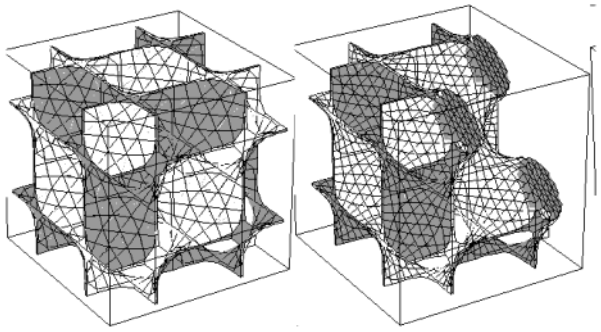

Figure 13. Triply periodic minimal surface from the Q_{II}^{D} phase (left), with a section removed to reveal part of a hexagonal array of ILAs (represented by the three "stumps" in the surface on the right). Again, the two sides of the surface have been shaded differently for clarity.

arrays of ILAs from one water region stack in an abc lattice. In fact, the Q_{II}^{D} phase may be thought of as ILAs from the two water regions occupying the same positions as Na^+ and Cl^- ions in an NaCl lattice, just as a Q_{II}^{P} phase consists of ILAs from the two water regions occupying the positions of Cs^+ and Cl^- ions in a CsCl lattice. (Note: Although our description of this process in Figure 12 might imply that the formation of a hexagonal array in two dimensions precedes the stacking of these arrays into a Q_{II}^{D} phase, in fact the processes probably occur concomitantly. The sequential description is shown in Figure 12 merely as an aid to visualizing the overall process.)

Finally, we suggest that the subsequent formation of Q_{II}^{G} from the intermediate Q_{II}^{D} occurs through a continuous deformation of the underlying TPMS. Such deformations can interconvert all three Q_{II} phases and have already been described as the final stage in the mechanism proposed by Siegel in section I. The transformation can occur without any tearing of the lipid bilayer if the TPMSs are related by the Bonnet transformation, although the Bonnet transformation is probably not itself the mechanism for the Q_{II} interconversion.[21] This requires that the lattice parameters are in the ratio $a(G)/a(D) = 1.58$.[41] It has been shown[41] that this is also the ratio at which the bending energies of the two phases are the same.

From the data from pressure jump experiments b and c, the positions of the intermediate peaks are consistent with a Q_{II}^{D} phase of lattice parameter $a(Q_{II}^{D}) = 138 \pm 1$ Å. This turns into a Q_{II}^{G} phase of approximate lattice parameter $a(Q_{II}^{G}) = 210 \pm 5$ Å. The ratio is $a(G)/a(D) = 1.5$, which is very close to the ratio predicted from the Bonnet relationship. Furthermore, we can use eq 3 to estimate the water volume fractions of the proposed Q_{II}^{D} and emergent Q_{II}^{G} phases from their lattice parameters. These are $\phi_w^D = 0.57$ and $\phi_w^G = 0.55$, respectively. Thus, if the intermediate structure is indeed Q_{II}^{D}, we would expect its free energy per lipid trimer to be close to that of the emergent Q_{II}^{G} phase, into which it could be converted with little bilayer tearing and little rearrangement of water. We suggest that this makes the Q_{II}^{D} phase a likely candidate for the intermediate in the L_α to Q_{II}^{G} transformation.

F. Jump from the L_β Phase. Finally, we turn our attention to the unusual behavior of the lamellar phase in the earlier stages of pressure jump experiment c (Figure 4c). As we have seen, the system starts in the L_β phase, where the stiffer bilayers cause the inter-bilayer repulsion to be much smaller than that in the L_α phase. The initial lattice parameter is $a = 58.10$ Å, in agreement with the equilibrium excess-water value of 58 Å,[42] which implies that not all of the water is incorporated between the bilayers.

Immediately after the pressure jump, the hydrocarbon chains melt, and the system changes into the L_α phase. This transition is too fast to be captured by the resolution of the experiment; previous measurements have shown its rate to be at least of the order of milliseconds.[43] The chain melting causes an immediate decrease in bilayer thickness and, therefore, also in lattice parameter. However, the bilayers now repel one another more strongly and take up the remaining water over the next 3.2 s, causing the lattice parameter to increase to a value of 64.06 Å, which corresponds to a water content of $\phi_w = 0.499$. This trend, however, is reversed by the formation of the Q_{II}^{G} phase, which sucks the water back out again, just as in the pressure jumps shown in Figure 4a and b.

We also note in passing the broadness of the L_α peaks immediately after the pressure jump. It has been suggested[44] that this reflects a P_β intermediate phase. Unfortunately, the beamline employed at the ESRF did not provide wide-angle data, so we cannot at the moment comment further on this possibility.

Acknowledgment. We wish to acknowledge the support of a Ph.D. student quota award from the EPSRC for A.S.

LA0259555

(41) Templer, R. H.; Seddon, J. M.; Warrender, N. A. *Biophys. Chem.* **1994**, *49*, 1−12.
(42) Squires, A. M. Bending Energetics and Phase Transition Kinetics in Type II Mesophases formed by Hydrated 2LA/DLPC. Ph.D. Thesis, Imperial College, 2002.
(43) Kriechbaum, M.; Laggner, P. *Progress In Surface Science* **1996**, *51* (3), 233−261.
(44) Quinn, P. Personal communication.
(45) http://www.esrf.fr/exp_facilities/ID2/handbook/ handbook/ beamline.htm#ID02.